[Frontiers in Bioscience 13, 3951-3965, May 1, 2008]

In silico study on the effect of F19T mutation on amyloid-β peptide (10-35)

Wei Han,[1] Hao Xiong[1], Yun-Dong Wu[1,2]

[1]Department of Chemistry, The Hong Kong University of Science & Technology, Clear Water Bay, Kowloon, Hong Kong, China, and [2]State Key Lab of Molecular Dynamics and Stable Structures, College of Chemistry, Peking University, Beijing, China

TABLE OF CONTENTS

1. ABSTRACT

The wild type (WT) amyloid-β (10-35) peptide, Aβ (10-35), and its F19T mutant have been studied by molecular dynamics simulations at 340 K in explicit water solvent each for over 3.4 μs. The WT peptide has a strong preference to form an E22-K28 loop (44% of total conformations) and a reasonable stability for a strand-loop-strand (SLS, L17-M35) (9%). The F19T mutant has a significantly lower population of E22-K28 loop (14%) and SLS structure (1.7%), but has a high population of Q15-D23 loop (48%). A specific interaction pattern among D23, V24, E22 and K28 was found to stabilize the E22-K28 loop in WT. Our results are in agreement with several experimental observations including: (1) the NOE constraints for the Aβ are reproduced; (2) the regions (15-23) and (22-28) can form loops; (3) the WT peptide is more structured than the F19T mutant. The current results also support our early proposal that the SLS structure might be important intermediate for monomer deposition to fibril, which explains the experimental fact that F19T mutant resists deposition to fibril.

2. INTRODUCTION

The formation of cerebral amyloid aggregates is characteristic of Alzeimer's disease (AD) (1,2). These aggregates, composed of amyloid-β (Aβ) peptides of 39-43 amino acids, are shown to be related to the pathogenesis of AD as they possess neurotoxicity (3-5). A possible way to develop drugs for AD would be therefore the inhibition of the formation of the Aβ aggregates (6-8). It becomes important to elucidate the mechanism of Aβ aggregation and the conformational features of all states involved in this process. It is of particular importance to know the conformational features of Aβ monomer, because the information about the monomer state may help to understand the aggregation mechanism and to design possible inhibitors (9,10). It has been recently found that soluble Aβ oligomers, intermediates between the Aβ monomer and the aggregates, are actually more toxic than the aggregates (11,12). The inhibition of the aggregates may even shift equilibrium of the Aβ peptides to the oligomers (11).

Several NMR experiments have been reported on monomer conformations of the Aβ and its fragments in

solution (13-19). Aβ (10-35) has been intensively studied among various Aβ fragments. Unlike full-length Aβ, it is more soluble, which allows clearer NMR observations about monomer conformations (13). Moreover, the Aβ (10-35) can deposit onto the aggregates formed by the full-length Aβ, indicating that the Aβ (10-35) could be a proper working model for the study of aggregation. Lee and co-workers proposed a collapsed coil (CC) structure for the Aβ (10-35) based on NMR NOE measurements (13,14). The CC has several turns in the middle of the peptide. The turns pack together and form a structured core.

There have been parallel efforts of molecular dynamics (MD) studies on the monomer conformations of the Aβ (20-30). The Aβ (10-35) has been studied by several groups (20,22-24). Straub and co-workers first probed the local dynamics of the CC with nanosecond-long simulations (20). We carried out microsecond-long simulations and found that the CC is dominant at room temperature at pH 5.6. But other conformations also exist (22). More recent replica exchange MD (REMD) simulations by Baumketner and Shea found similar phenomenon (24). Interesting, our simulations indicate the existence of a strand-loop-strand (SLS) structure for the Aβ (10-35) monomer at the room temperature. More importantly, this SLS structure exists under other conditions such as high temperature (400 K) and protonated E22 and D23 that mimic E22N and D23Q mutations (22). Under these conditions, the CC structure becomes unstable and disrupted. The SLS structure has a loop (E22-K28) and two strands (L17-A21 and A30-M35). The two strands contact with each other in an anti-parallel fashion. We therefore proposed that the SLS structure might be an important intermediate for monomer deposition to aggregates (22). This seems to be in line with the finding by Lazo *et al* that Aβ (21-30) exists as a loop structure in aqueous solution (19). Mastrangelo *et al* also found by AFM experiment that Ab (1-42) monomer exists as an SLS structure on silicon surface (31).

Associated with the NMR studies on the Aβ (10-35), it was found that the NOE signals of the Aβ correlate with its ability of depositing onto aggregates (13,15,16). A mutation, F19T, can change the signals and essentially prevent the Aβ from deposition. A similar observation of F19T mutation effect was also reported for Aβ(1-42) (32). This mutation takes place in L17-21, the central hydrophobic core (CHC). Although detailed structure could not be derived, Maggio and coworkers indicated that the mutation significantly increases the conformational flexibility of the peptide. They suggested that there could be certain deposition-active conformations, the loss of which may account for the reduction in deposition rate for the F19T mutant (15,16,33). Using a predictive algorithm, Dobson *et al* were able to correlate the loss of deposition ability of the F19T mutant with the decrease of hydrophobicity and the β-sheet propensity of the CHC (34). However, an understanding of the above phenomenon at a molecular level is lacking. It would be very useful to make a comparison of conformational features between the wild type (WT) Aβ and the F19T mutant through molecular dynamics simulations.

To this end, we have carried out long MD simulations for both WT Aβ (10-35) and its F19T mutant up to 3.5 μs for each in explicit solvent at optimal deposition temperature of 340 K (35). In this paper we would like to (1) make a comparison in conformational features between WT Aβ (10-35) and its F19T mutant; (2) analyze the various factors that contribute to the conformational difference, especially specific pattern of side chain interactions in important conformations and topologies of the Aβ; (3) to provide a rationalization of reduced deposition of F19T mutant.

3. METHODS AND MATERIALS

3.1. MD simulations

All MD simulations were performed with the GROMACS 3.2 software (36). The initial conformation of the WT simulation was taken from the first one of the conformations from the NMR experiments (PDB code: 1HZ3) (14). This conformation was also used as the initial conformation of the F19T simulation except that the Phe19 was mutated into a Thr. To mimic the experimental pH conditions, the ionizable groups of His and Lys are protonated and the ionizable groups of Asp and Glu are deprotonated (14). The WT or F19T peptide was put into a dodecahedron box. The peptide is at least 1.1 nm distant from any edge of the box. About 2,600 molecules of single-point charge (SPC) water were filled in the box (37). Two chloride ions were added to neutralize the systems. All bond lengths of the peptides were constrained by the LINCS algorithm (38). Geometry of water was constrained by the SETTLE algorithm (39). A cut-off of 1.0 nm was applied to non-bonded interactions. Electrostatic interactions were treated by the reaction field method with a dielectric constant of 78 beyond the cut-off (40). The previous studies of another group and ours suggested that the reaction field method can reasonably consider electrostatic interactions of Aβ peptides in water (24,41). In addition, we used a time step to 5 fs by increasing mass of hydrogen to 4 a.u. and by using dummy atoms. It has been demonstrated that this does not perturb thermodynamics and dynamics of the systems (22,42).

All simulations started with a 2,000-step minimization, followed by a NPT pre-equilibrium simulation with positions of peptide atoms constrained. The NPT production simulations were thereafter performed. Conformations are recorded every five ps. Simulation temperature and pressure were kept constant at 340 K and 1.0 atm by an external thermostat and a pressure bath with coupling constants of 0.1 and 1.0 ps, respectively (43).

3.2. Calculations of intramolecular contacts

Three kinds of intramolecular contacts were analyzed. First, the contacts between the C_α atoms of different residues were investigated. Residue *i* and *j* are considered to have a C_α contact if the distance between the two C_α atoms is less than 0.65 nm. Then a C_α contact map can be constructed with the point (*i*, *j*) on the map representing the probability of the residues *i* and *j* having a C_α contact. For a peptide, the patterns on its C_α contact map can reflect its overall topology.

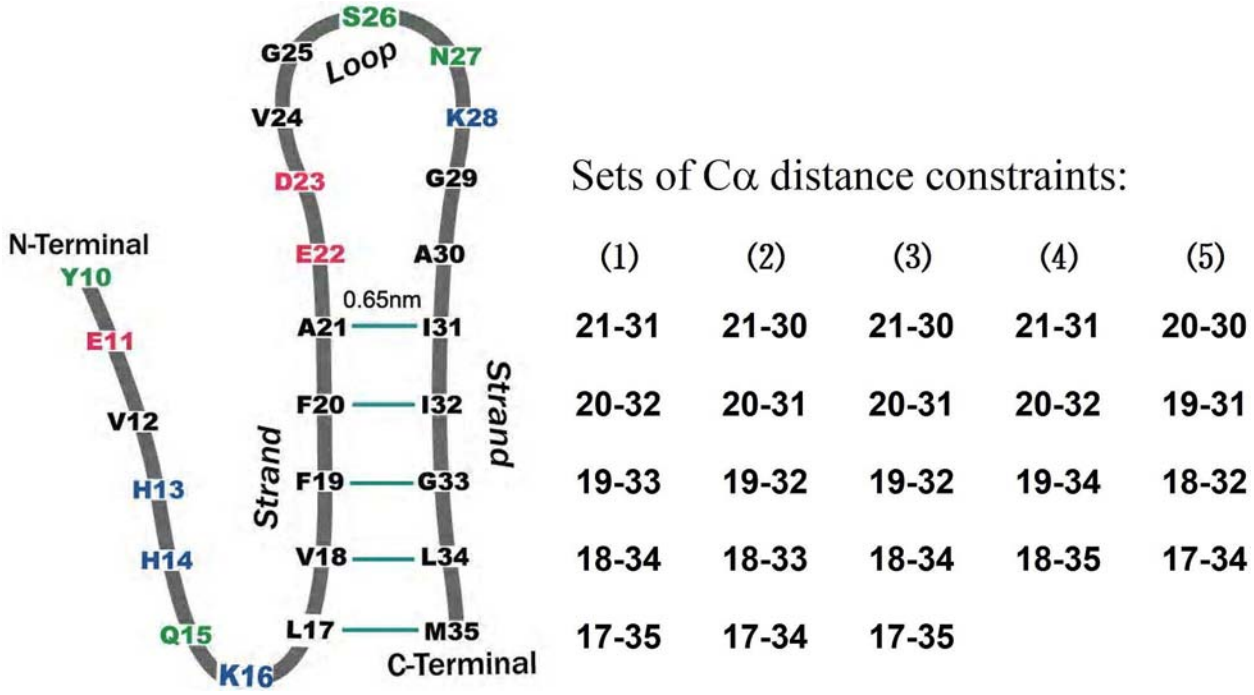

Figure 1. Scheme of the sets of C_α constraints between L17-A21 and A30-M35 for defining the SLS structures.

Second, the number of the atomic contacts between two groups of atoms was computed with a cut-off distance of 0.54 nm. The contact number may indicate the interaction strength between two groups if the interaction originates from a van de Waals interaction or a hydrophobic interaction.

Third, the contacts associated with hydrogen bond (HB) interactions were calculated. If the *D* atom of a proton-donor group (*D-H*) is closer than 0.35 nm to the A atom of a proton-acceptor group (*A*), and if the angle *D-H-A* is greater than 120^o, then these two groups are considered to have an HB contact.

Finally, we also analyzed salt bridge contacts for ionic side chains of Lys, Asp and Glu. The salt bridges have been studied for the Aβ in previous studies (22-24,41). Unlike an HB, a salt bridge is basically a charge-charge interaction and can be considered as spherical. Therefore, if O of a carboxylic group and N of an ammonium group are closer than 0.5 nm, the two groups are considered to have a salt bridge contact, the same as we did before (22).

3.3. Identification of a reverse loop

Finding a reverse loop in the Aβ (10-35) is one of our major tasks during the conformational analysis. To identify a reverse loop from the simulated conformations, the C_α contacts between the residues i and j and between the residues *i*+1 and *j*-1 are investigated. The simultaneous presence of both two contacts in a conformation can indicate that there is a possible loop spanning from the residue *i* to the residue *j* and this loop has its two terminals in an anti-parallel arrangement.

3.4. Identification of the SLS

We previously defined the SLS according to sets of the *i-j* C_α contacts (22). The similar sets of the C_α contacts are applied to the identification of the SLS in this study. A conformation can be considered to have the SLS topology only if it has a reverse loop spanning 22-28 (Section 3.3), and satisfies any set of the *i-j* C_α distance constraints (<0.65 nm) that are shown in Figure 1.

3.5. Conformational Clustering

The conformational clustering was carried out by the root mean square deviation (RMSD) of atom distances (44). If a set of selected atoms is chosen for a comparison between two conformations *a* and *b*, the distance d_{ij} between any pair among this set of atoms is calculated. The RMSD between those two conformations will be

$$\sqrt{\frac{\sum_i \sum_{j>i} \left(d_{ij}^a - d_{ij}^b\right)^2}{n(n-1)/2}},$$

where *n* is the number of the selected atoms. If the RMSD falls within a certain cut-off, the conformations *a* and *b* may belong to the same cluster in regards to the chosen atoms.

4. RESULTS

4.1. The simulations are close to equilibrium and the results are consistent with NMR experiments

It is important to examine first if the sampling is adequate. We performed the conformational clustering for the WT and the F19T simulations according to all the C_α

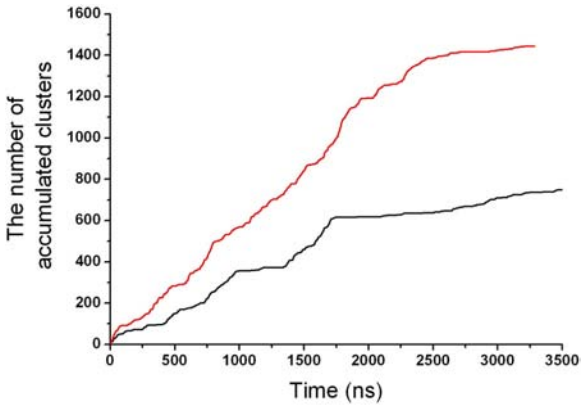

Figure 2. The numbers of accumulated clusters sampled during the WT (black) and F19T (red) simulations.

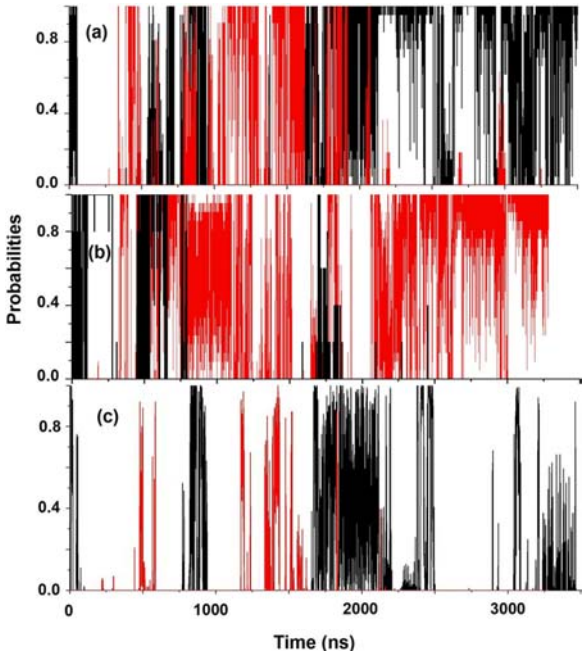

Figure 3. The probabilities of Loop 22-28 (a), Loop 15-23 (b) and the SLS (c) in the WT (black) and F19T (red) simulations. (a) and (b) take an adjacent average over 20 neighboring data points. (c) takes an adjacent average over 50 neighboring data points.

atoms as described in Section 3.5. The clustering cut-off is 0.2 nm. As shown in Figure 2, the numbers of accumulated clusters sampled appear to level off at the ends of the WT and F19T simulations, implying that the two simulations may be close to equilibrium. Moreover, the sampling of certain topologies in the Aβ (10-35) was also investigated. Three topologies, a loop 15-23, a loop 22-28 and a strand-loop-strand (SLS), are our primary interests (Section 4.2 and 4.7). As demonstrated in Figure 3, all these topologies fold and re-fold for many times during the WT and the F19T simulations. This suggests that the sampling of these structures may be adequate.

Another important matter is to which extent the simulations can reproduce experimental observations. For the WT Aβ (10-35) in water, Lee and co-workers have reported thirty long range NOE constraints with NMR spectroscopy, from which the collapsed coil (CC) was derived (14). The upper bounds of these NOE constraints are shown in Figure 3. We therefore calculated the inter-proton distances corresponding to those NMR constraints. An inter-proton distance is computed as $\langle d^{-6} \rangle^{-1/6}$, an average over all the conformations. The distances for the WT simulations are listed in Figure 3. Among the thirty constraints, seventeen are fully satisfied, eight are weakly violated (by less than 0.1nm) and two by 0.1 to 0.2 nm. Only three of them are strongly violated (by more than 0.2 nm). Shea and co-workers recently performed the same NOE analysis based on their REMD simulations of the Aβ monomer (24). The consistence of our results with experiment is comparable to theirs.

Due to a lack of experimentally assigned NOE data, a similar analysis was not carried out for the F19T simulation. However, an expanded NOESY spectrum indicates that the cross-coupling signals involving the aromatic protons are much fewer in the F19T than in the WT (13), suggesting that the F19T is less ordered (15). We computed the contact numbers of the aromatic carbons of F19 and F20 with all the other sidechain carbons carrying hydrogen atoms. In the WT, F19 and F20 have on average 22.1 and 21.4 contacts, respectively; In the F19T mutant, F20 has only an average of 14.6 contacts. In addition, the F19T simulation samples 1,444 clusters and the WT simulation sampled 748 clusters in the same amount of time, indicating that the F19T mutant is more flexible and less structured, in qualitative agreement with the experiments (13,15).

4.2. The analysis of overall topologies reveals that the WT favors Loop 22-28 and the F19T mutant favors Loop 15-23

The map of the probabilities of the C_α contacts (Section 3.2) in the Aβ (10-35) was built over 0.7 million conformations collected in the WT simulations (Figure 5, top). Although the clustering results suggest that there is no single cluster with a probability greater than 3%, the C_α contact map clearly shows that there are three main loop topologies along the WT Aβ (10-35), as indicated by the C_α contact bands which are vertical to the diagonal of the map.

First, the contact band in Box *I* (Figure 5, top) indicates that the Aβ (10-35) favors reverse loops (Loop *I*) around E22-K28 with a turn around G25. This is in accord with the experimental findings that E22-K28 has a high loop propensity (19). It also agrees with our previous calculation (22). The band in Box *II* indicates that there is another loop (Loop *II*) roughly spanning Q15-D23 with a bend around L17-F20. Additionally, a third loop (Loop *III*) is found around N27-A30. It is minor compared to the first two loops. The observations of the bends around L17-20 and the loops around N27-A30 are consistent with the structures from experiments (14).

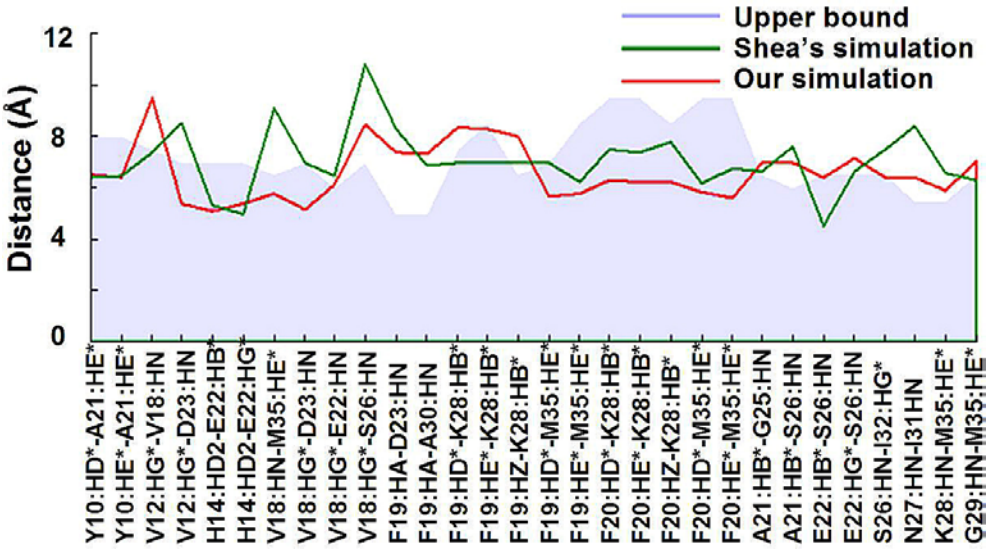

Figure 4. The 30 long-range NOE distances derived from NMR experiment (gray area, ref. 14), calculated from the REMD simulations (green lines, ref. 23) and ours simulations (red lines).

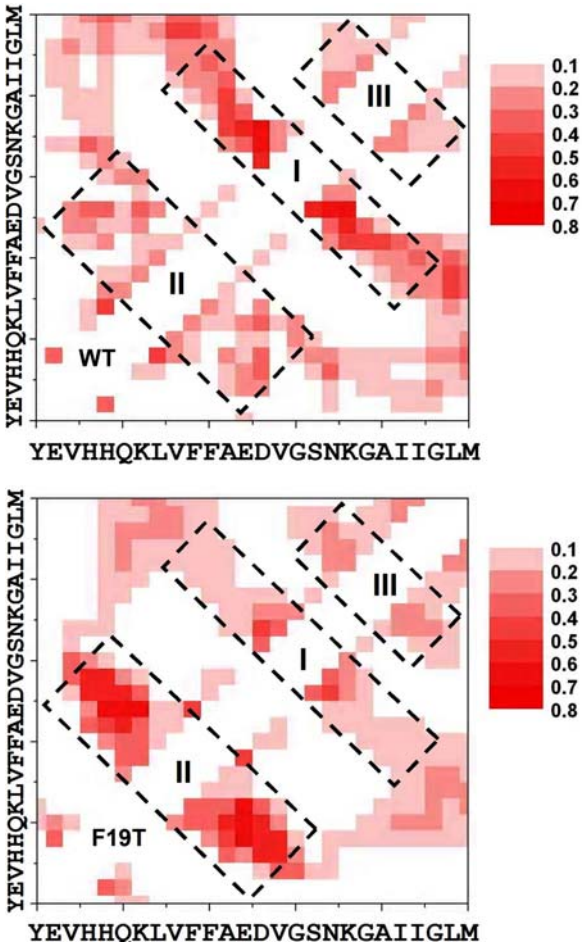

Figure 5. The maps of the Ca contacts of the WT and the F19T simulations. Boxes with dashed edges indicate the contact bands that correspond to loop regions in the Aβ (10-35).

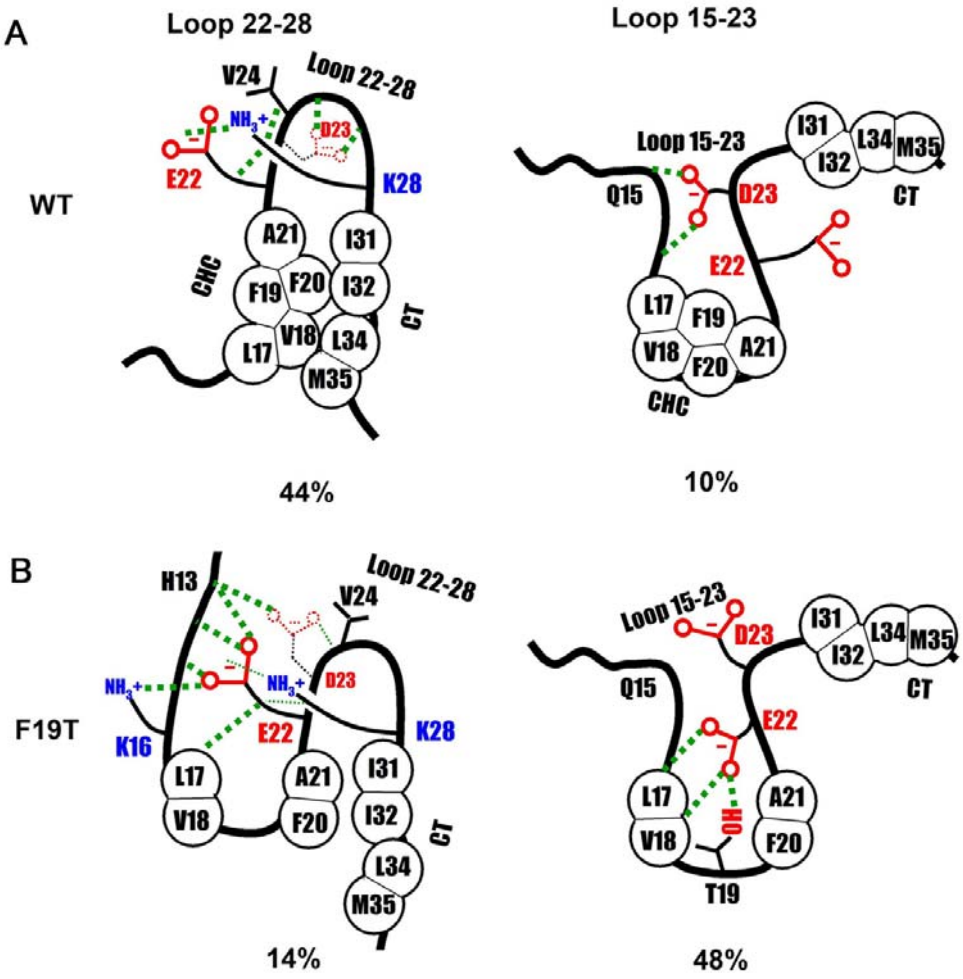

Figure 6. Schematic representations of the loops 15-23 and 22-28 in the WT and the F19T mutant. The beads depict hydrophobic residues. The thick green dash lines and the thin green dash lines represent the strong and the weakened interactions involving the side chains of E22, D23, V24 and K28, respectively. The number below each structure indicates the population of this structure.

The C_α contact map for the F19T mutant was also constructed in the same way (Figure 5, bottom). The three loop regions found in the WT are still present in the F19T mutant except that the probability of Loop *I* is greatly reduced and the probability of Loop *II* is significantly enhanced.

Loop *I* or *II*, which is indicated by the C_α contact maps, is actually a collection of similar loop structures. An explicit definition of Loop *I* or *II* is needed to estimate the loop population. We defined Loop *I* as a group of conformations with a loop exactly spanning E22-K28, namely the loop 22-28. The loop 22-28 can be identified as described in Section 3.3. This definition can lead to the highest population of Loop *I* among all the other possible definition of Loop *I*. Similarly, a loop exactly spanning Q15-D23 is used to define Loop *II*. Schematic views of the loops 15-23 and 22-28 of the WT and the F19T mutant are displayed in Figure 6. The probabilities of the loops 15-23 and 22-28 for the WT are computed to be 0.10 and 0.44, respectively while the same probabilities for the F19T mutant are 0.48 and 0.14, respectively. These data suggest that the WT favors Loop 22-28 while the F19T mutant favors Loop 15-23.

4.3. The analysis of electrostatic interactions reveals the importance of the interactions between the E22 and D23 side chains and peptide backbone

Electrostatic interactions are one important factor that render the Aβ (10-35) ordered structure (13,14). There are four kinds of electrostatic interactions including hydrogen bonds (HB) between backbone amide groups, HBs between polar side chains, salt bridges between charged side chains and HBs between side chains and backbone. All four types are analyzed according to Section 3.2.

The analysis reveals that HBs between backbone amide groups are weak in both the WT and the F19T mutant. Most of these HBs are less than 10% and none of them is more than 20%. Table 1 summarizes the probabilities of the HBs between the polar side chains of the Aβ. All the HBs are

Table 1. The probabilities (%) of hydrogen bonds between polar side chains for the WT and the F19T mutant[1]

	E11[2]		**E22**[2]		**D23**[2]	
	WT	F19T	WT	F19T	WT	F19T
Y10[3]	0.2	0.1	15.7	5.3	5.6	1.6
H13[3]	**33.1**[5]	**53.2**	9.4	6.9	23.2	19.6
H14[3]	**32.2**	16.7	6.0	16.9	**30.5**	**44.3**
Q15[3]	2.4	1.0	0.7	2.8	1.5	3.9
K16[4]	8.7	1.0	14.5	12.7	2.6	17.7
F(T)19[3]	0.0	0.0	0.0	26.0	0.0	0.1
S26[3]	3.4	1.1	0.4	1.8	7.7	7.0
N27[3]	3.7	0.7	2.3	2.3	6.6	13.1
K28[4]	2.3	1.8	15.3	4.6	**20.0**	3.8

Abbreviations: The probabilities related to Q15 and N27 are not listed as they are all lower than 3%;[1] HB acceptors;[2] HB donors. An HB between a donor (*A*-*H*) and an acceptor (*D*) is considered to form if *D* and *A* are closer than 0.35 nm and the angle *O*-*H*-*A* is greater than 120°;[3] Only salt bridges between Lys and Asp or Glu are considered as all the HBs between them are less possible than 3%, and a salt bride between a carboxylic group and an ammonium group is considered to form if any O atom of the carboxylic group and the N atom of the ammonium group are closer than 0.5 nm;[4] The probabilities greater than 20% are highlighted in **bold**.[5]

weak in the WT except for those involving the side chains of H13, H14, E11 and D23. The E11 side chain favors HBs with the H13 and H14 side chains and the D23 side chain favors HBs with H13 and H14. Their probabilities are greater than 0.2. Our findings are in accord with the NMR experiments where the only observable NOE signals between polar side chains are those among Asp, Glu and His (13,14). The F19T mutation basically has little effect on side-chain HBs of the Aβ except for the HBs between E11 and H13 and between E22 and T19.

Table 1 also listed the probabilities of the salt bridges involving E22, D23, K16 and K28. E22 forms a salt bridge with K16 and K28, respectively, to a similar extent. D23 is more likely to form a salt bridge with K28 than with K16. However, no salt bridge has an average probability greater than 0.2. The F19T mutation disfavors the E22-K28 and D23-K28 salt bridges but enhances the E22-K16 and D23-K16 salt bridges

Finally, we analyzed all possible HBs between polar side chains and backbone amide groups. Most HBs of this sort are weak (<10%) in both the WT and the F19T mutant except for the HBs involving the side chains of E22 and D23. The probabilities related to E22 and D23 are shown in Figure 7. In the WT, the D23 side chain favors HBs with two parts of the backbone, Q15-L17 and G25-S26. The probabilities range from 0.2 and 0.4. On the contrary, the E22 side chain has no detectable HBs with the backbone. In the F19T mutant, E22 becomes more likely (0.42-0.52) to have HBs with the L19-T19 backbone but the HBs between the D23 side chain and the Q15-L17 backbone are weakened.

4.4. The F19T mutation breaks the central hydrophobic core (CHC) and weakens the interactions between the CHC and the C-terminal (CT)

The central hydrophobic core (CHC) (13) fragment L17-A21 and the C-terminal (CT) fragment A30-M35 are known to play key roles in the Aβ (10-35) folding. By calculating the average numbers of atomic contacts, we measured the strength of the hydrophobic interactions among the sidechains of the CHC and the CT (Section 3.2), which are given in Figure 8 and 9**.**

As shown in Figure 8, in the WT the sidechains of the CHC forms a compact core. F19 appears to be critical for the intactness of this core. Its contact numbers with its two adjacent residues, V18 and F20, are about 5.5 and 4.7, respectively. Besides, the side chains of L17 and L18 have considerable interactions with the side chains of F20 and A21. Upon the F19T mutation, the compact core is disrupted, as indicated by the reduction in the contact numbers between L17/V18 and F20/A21, and between the residue 19 and its adjacent residues. In the meanwhile, the V17-L18 and F20-A21 interactions are significantly enhanced. Therefore, the compact core is actually broken into two separated parts, L17-V18 and F20-A21. This coincides with the experimental fact that the F19T mutation in Aβ (10-35) can change the folding characteristics of the CHC (15,16). As expected, similar analysis indicates that for the WT and the F19T mutant, the mutation has little effect on these hydrophobic interactions in the CT fragment (data not shown).

We also investigated the hydrophobic interactions between the CHC and the CT (Figure 9). In the WT, considerable interactions are found between the CHC and the CT. In particular, F19 and F20 in the CHC prefer interactions with the CT, and L34 and M35 in the CT prefer interactions with the CHC. In the F19T mutant, the residue T19, which is hydrophilic, does not have strong interactions with the CT fragment. V18 and F20, adjacent to T19, also have their interactions with the CT reduced.

Table 2 summarizes the total numbers of hydrophobic contacts of the CHC and the CT and between the CHC and the CT. After the F19T mutation, the overall number of contacts decreases by about 11 because of the disruption of the compact core in the CHC and the weakening of the CHC-CT interactions.

4.5. Structures and stabilities of Loop 22-28

The calculated probability of the loop 22-28 is 0.44 for the WT and 0.14 for the F19T. To understand the

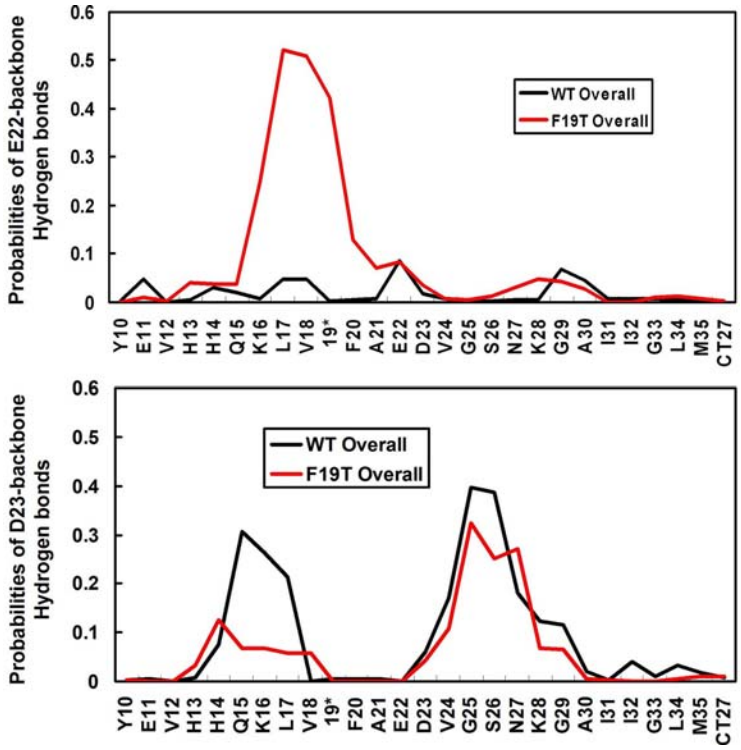

Figure 7. The probabilities of forming hydrogen bonds between backbone amide groups and the side chain of E22 (top) or D23 (bottom). The red lines indicate the probabilities from the WT simulation; the black lines indicate the probabilities from the F19T simulation.

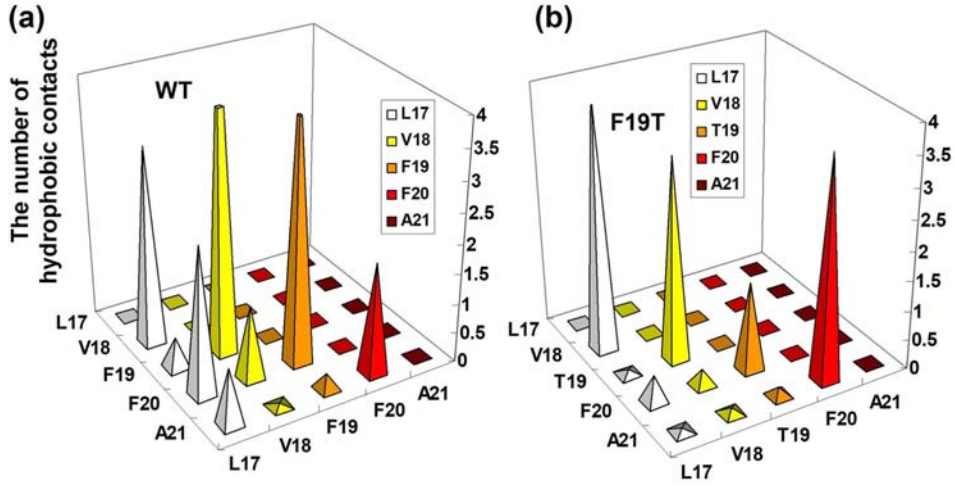

Figure 8. The average numbers of hydrophobic contacts between the side chains of the central hydrophobic core (CHC) fragment for (a) the WT and (b) the F19T simulation.

stability of this loop, it is necessary to look into the structures of this loop and the stabilizing forces for the structures. To do so, we gather all the conformations with a loop 22-28 (Section 3.3) as an ensemble, namely the loop 22-28 ensemble. The ensemble was clustered according to the side-chain heavy atoms of E22-K28 with a cut-off of 0.15 nm (Section 3.5). In addition, both electrostatic and hydrophobic contacts were analyzed for the ensemble as were done in Section 4.3 and 4.4.

The clustering for the WT leads to the three most populated clusters that account for about 75% of the population of the ensemble. Interestingly, all of them have a very similar pattern of side-chain interactions as shown in

Table 2. The average numbers of hydrophobic contacts in the central hydrophobic core (CHC) fragment L17-A21 and the C-terminal (CT) fragment A30-M35 and between the two fragments for the WT and the F19T mutant

	CHC	CT	CHC-CT	Sum
WT	19.3	9.5	22.1	50.9
F19T	13.9	10.5	15.1	39.5

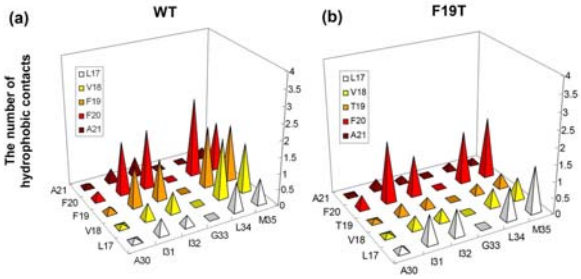

Figure 9. The average numbers of hydrophobic contacts between the side chains of the central hydrophobic core (CHC) and the C-terminal (CT) fragments for (a) the WT and (b) the F19T mutant.

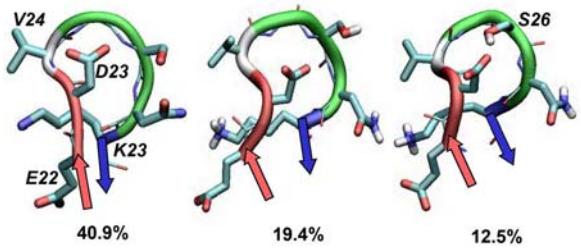

Figure 10. The most populated clusters of the loop 22-28 ensemble of the WT. The arrows indicate the directions of the termini of the fragment 22-28. The number below each structure is the population of the structure in the loop 22-28 ensemble.

Figure 6a and 10: 1) the D23 side chain lies on one side of the loop plane and forms HBs with the G25-S26 backbone; 2) the E22, V24 and K28 side chains are on the other side; 3) E22 and K28 form a salt bridge; 4) the E22 and V24 side chains clamp the K28 side chain through hydrophobic interactions. This pattern is also supported by the data from the contact analysis for the ensemble. The loop ensemble has a probability of about 0.6 and 0.7 to have HBs between the D23 side chain and the G25 and S26 backbone, respectively. These probabilities are higher than the overall probabilities shown in Figure 7, indicating that the HBs between the D23 side chain and the G25-N26 backbone are especially favored in the loop 22-28. In the loop ensemble, the chance to form a E22-K28 salt bridge is about 0.33. But none of the E22-K16, D23-K16 and D23-K28 salt bridges can be found. The analysis on hydrophobic interactions also reveals that the contact numbers between E22 and K28 and between V24 and K28 are 3.7 and 1.8, respectively. These interactions are two of the strongest hydrophobic interactions in the loop ensemble.

In contrast to the WT, the structures of loop 22-28 in the F19T mutant become more diversified and have no dominant interaction pattern. Only the most stable cluster has a similar pattern to that in the WT. This cluster accounts for about 30% of population of the ensemble. The probabilities of HBs between the D23 side chain and the G25-S26 backbone drop by about 0.15-0.2. The probability of the E22-K28 salt bridge also decreases by about 0.2. Besides, the contact numbers between E22 and K28 and between V24 and K28 are 1.9 and 1.2, respectively. Interestingly, the F19T mutation introduces several new interactions into the loop 22-28 ensemble. For example, both E22 and D23 are able to form a salt bridge with K16 (probabilities of about 0.2). The E22 side chain can form HBs with the H13-H14 and L17-F20 (probabilities of 0.2). Additionally, the total number of hydrophobic contacts between E22 and the region H13-F20 increases by about 6.0 from the WT to the F19T mutant.

Taken together, the above analysis suggests that the reduction in the population of the loop 22-28 correlates with a loss of a special pattern of side-chain interactions involving E22, D23, V24 and K28. The loss of the pattern due to the mutation is accompanied with a gain of the interactions of E22 and D23 with H13-F20. The gain can be understood since the F19T mutant favors the loop 15-23, which can bring H13-F20 to E22 and D23. Therefore, it appears that the presence of the loop 15-23 can interfere with the stability of the loop 22-28.

4.6. Structures and stabilities of loop 15-23

Similar clustering and contact analysis were carried out for the loop 15-23 ensemble, which includes all the conformations with a loop spanning 15-23. The ensemble was clustered according to the side-chain heavy atoms of Q15-D23 and the cut-off was set to 0.2.

The most populated loop clusters in the WT are shown in Figure 11a. Clearly, most of the clusters have a hydrophobic compact core composed of the L17-A21 side chains despite that the structures of the clusters are diversified. In particular, the F19 side chain is in the center of the core in most of the clusters. A visual inspection on the clusters with the core also reveals that the amide hydrogen of the L17-F19 backbone is shielded by the core. In addition to hydrophobic interactions, other kinds of interactions, such as those between the D23 side chain and the Q15-K16 and between E22 and K28, can also be found.

As shown in Figure 11b, upon the F19T mutation, the compact hydrophobic core in the CHC fragment is disrupted, which is consistent with our analysis of hydrophobic interactions in the F19T in Section 4.4. Without the hydrophobic core, the L17-T19 backbone becomes more exposed. The exposure allows the E22 side chain to form HBs with the L17-T19 backbone. In addition, the F19T mutant forms a HB (a probability of about 0.37) between the side chains of E22 and T19 in the loop 15-23. Thus, it appears that the aforementioned HBs involving E22 correlate with the stability of the loop 15-23.

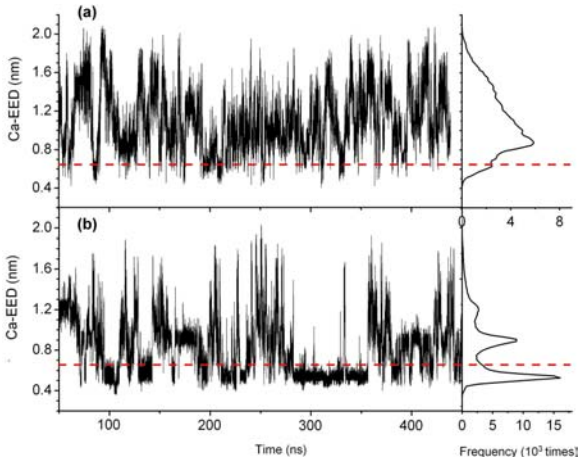

Figure 11. The most populated clusters of the loop 15-23 ensemble of (a) the WT and (b) the F19T mutant. The arrows indicate the directions of the termini of the fragment 15-23. The number below each structure is the population of the structure in the loop 15-23 ensemble.

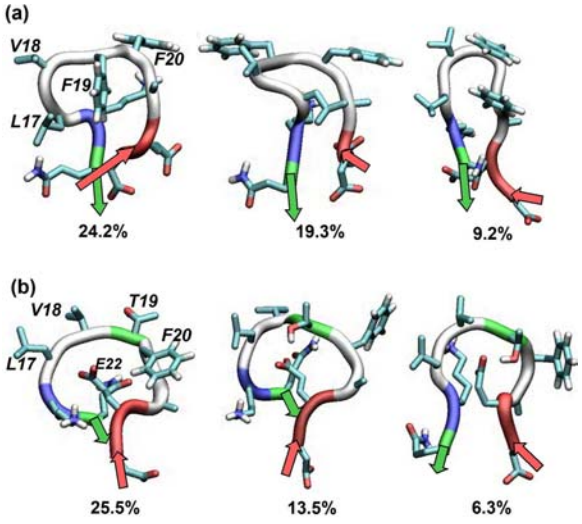

Figure 12. The distances between the C_α atoms of K16 and E22 from (a) the WT (a) and (b) the F19T simulations with the OPLS-AA/L force field and the TIP3P water. The graphs on right are the distributions of the distances. The red dashed lines indicate distances of 0.65 nm.

Since the F19T mutation promotes Loop 15-23 and which in turn affects the folding of other part of the peptide, it is important to examine if the increased stability of Loop 15-23 depends on the simulation protocol. We therefore performed a 500 ns simulation (340 K) for each of the WT fragment, Ac-Q_{15}KLVFFAED$_{23}$-NH_2, and its F19T mutant with the OPLS-AA/L force field (45) and the TIP3P water model (46). Electrostatic interactions were treated with the particle-mesh Ewald (PME) method (47). The distances between the C_α atoms of K16 and E22 are shown in Figure 11. It is clear that the F19T mutation (Figure 12b) increases the K16-E22 C_α contact (Figure 12a), as indicated by the contact probabilities of 0.06 (WT) and 0.39 (CHC). This analysis indicates that our observation about the loop 15-23 does not depend on the simulation methods.

4.7. Structures and stabilities of the SLS

We finally tried to analyze the propensity of the Aβ (10-35) to form the SLS structures. We picked up the conformations with a SLS topology by the methods as described in Section 3.4. Our definition of the SLS intends to allow L17-A21 and A30-M35 to be arranged in an anti-parallel fashion and have as many C_α contacts as possible between hydrophobic residues. This leads to a SLS probability of 8.7% in the WT, which is similar to the SLS probability that we derived before (22). The representative structures of the SLS ensemble reveal that L17-A12 and A30-M35 indeed strongly interact with each other (Figure 13). The SLS probability in the F19T mutant is only about 1.7% much lower than in the WT, suggesting that the mutation greatly destabilizes the SLS.

The destabilization of the SLS by the F19T mutation may be understood as follows: 1) the SLS possesses the loop 22-28 while the loop 22-28 is destabilized by the F19T mutation; 2) the mutation severely weakens the interactions between the CHC and the CT. The analysis of hydrophobic interactions shows that the overall number of contacts between the CHC and the CT is about 30 in the WT, but is reduced to about 19 in the F19T mutant.

5. DISCUSSIONS AND CONCLUSSIONS

5.1. Intrinsic stability of the loop 22-28 in the WT Aβ peptide

One important issue that we attempt to address here is if the Aβ monomer is likely to have any obvious conformation or topology, and what are the features of the conformation or topology. Our simulation of the WT Aβ revealed that a loop spanning E22-K28 has a population of about 44% (Figure 6a, left). A loop that spans Q15-D23 has a moderate stability (10%) (Figure 6a, right). Our findings agree with recent observation that the fragment Aβ (21-30) adopts a reverse loop structure (19). Besides, the Aβ structures derived from NMR experiments also have a loop around Q15-D23 (14).

More importantly, a dominant pattern of side-chain interactions is found in the loop 22-28, which is clearly shown in Figure 6a. In the loop 22-28, the D23 side chain is on one side of the loop plane while the E22, V24 and K28 sidechains are on the other side. D23 form a strong HB with the G25-S26 backbone. E22 and K28 form a salt bridge. The hydrophobic moieties of E22, V24 and K28 also have considerable interactions with each other. Previous experimental (19) and theoretical (27) studies have intensively investigated the side-chain interactions of the region 22-28. From ROE measurements, Lazo *et al* found that the Aβ (21-30) favors a hydrophobic interaction between V24 and K28 and a moderate electrostatic interaction between K28 and E22 or D23 (19). Through REMD simulations of the Aβ (21-30), Baumketner *et al* found that D23 prefers HBs with the G25-K28 backbone than an electrostatic interaction with K28. They found no

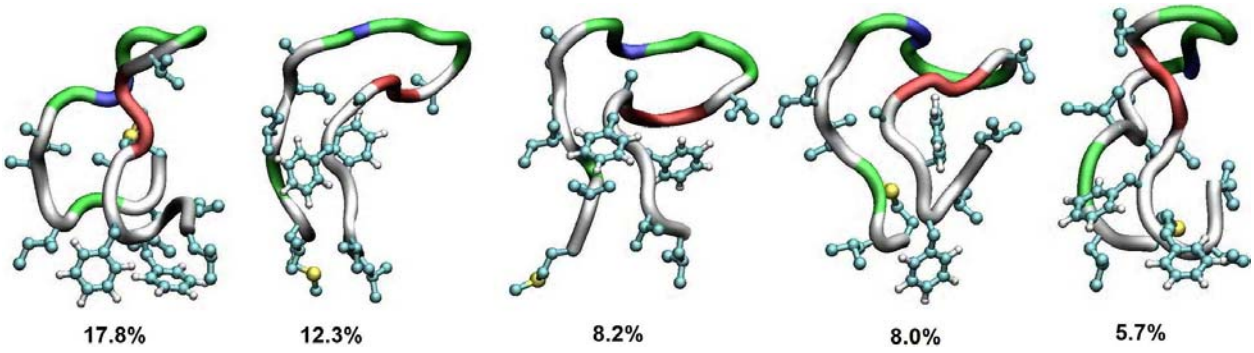

Figure 13. The most stable clusters of the SLS ensemble and their population in the ensemble (the numbers below). They were clustered according to the side-chain heavy atoms of the regions L17-A21 and A30-M35 with a RMSD cut-off of 0.25 nm.

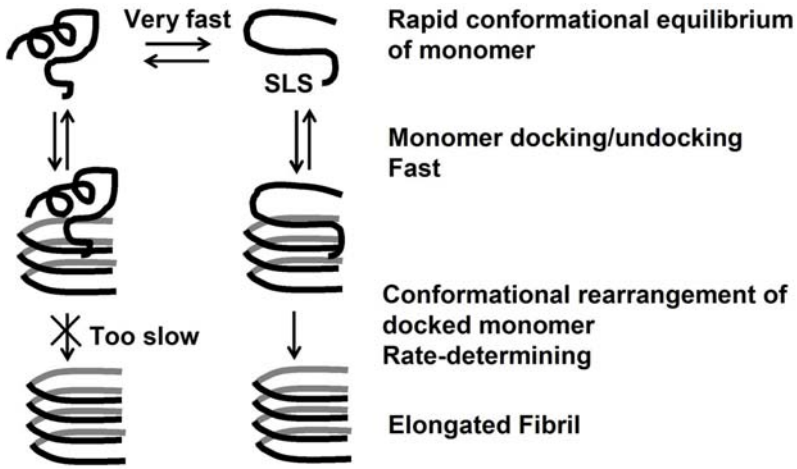

Figure 14. Scheme of the dock-lock model of fibril elongation by deposition of Aβ monomer and the possible role of the SLS in the elongation.

interaction between V24 and K28 was found (27). Thus, our simulation results account for most interactions in the loop 22-28 that were separately reported for the WT.

5.2. Significant changes in Aβ conformation by F19T mutation

In our simulations, the F19T mutation greatly enhances the population of the loop 15-23 but significantly decrease the chance of the loop 22-28 (Figure 6b). The enhancement of the loop 15-23 by the mutation may be due to two reasons. In the WT, the L17-A21 side chains form a compact core and shield the L17-F19 backbone. However, the mutation breaks the core and makes the L17-T19 backbone more exposed, which allows strong HBs between the E22 side chain and the L17-T19 backbone. In addition, the hydroxyl group of T19 is likely to form a HB with the E22 side chain.

Since the mutation happens inside the region 15-23, its effect on the stability of the loop 15-23 is straightforward. Nevertheless, what causes the population reduction of the loop 22-28? Our analysis reveals two possible causes. (1) The stabilizing interactions in the loop 22-28 may be interfered by the formation of the loop 15-23. Once the loop 15-23 is formed, the region H13-F20 can come close to E22 and D23 that play important roles in the stability of the loop 22-28. (2) The mutation weakens the interactions between L17-A21 and A30-M35. Since the two regions flank the region E22-K28, they can bring two termini of the region 22-28 together and help to close the loop once they are in close contact.

5.3. Possible roles of D23-K28 salt bridge and E22/D23-bakbone hydrogen bonds in the Aβ folding

An interesting finding from our simulations is that there is only a moderate salt bridge interaction between D23 and K28 although this salt bridge is known eventually to form in the aggregates according to experiments (48,49). The salt bridge is weak in our simulation, which agrees with ROE experiments (19) and a recent MD study on the Aβ (10-35) (23). Furthermore, we found that the loop 22-28 in particular disfavors the D23-K28 salt bridge. A REMD study also observed the similar phenomenon (27). Therefore, the D23-K28 salt bridge may not be the major electrostatic interaction that determines the folding of the Aβ monomer and the intrinsic propensity of the loop 22-28.

Instead, our systematic analysis showed that the HB interactions between the side chains of E22 and D23 and the peptide backbone are more important, and very

sensitive to the F19T mutation. Moreover, E22 and D23 take part in quite different interactions despite that they have similar side chains and are adjacent in the sequence. In the WT, the D23 side chains form HBs with the Q15-L17 and G25-S26 backbone but E22 basically forms no HBs with the backbone. In the F19T mutant, the E22 side chain favors HBs with the L17-T19 backbone in the F19T mutant while the D23-backbone interactions are slightly decreased.

Our results of E22/D23-bakcbone electrostatic interactions agree with several experimental observations: (1) NMR experiments (13,14) have shown that the Aβ (10-35) changes its conformation with pH value increasing from 2 to 5.6, indicating that the anionic sidechains of E22 and/or D23 may play roles in the Aβ folding. However, a pK_a study showed that the pH dependence of the Aβ monomer does not rely on salt bridge interactions (50). The E22 and D23 side chains may be involved in other types of electrostatic interactions; (2) NMR experiments observed the NOE coupling between C_β-H of D23 and N-H of G25 (14), indicating a possible HB between the D23 side chain and the G25 backbone; (3) an inspection on the conformations derived from NOE signals (13,14) shows that the D23 side chain can from HBs with the Q15-L17 backbone; (4) another NMR study showed that an E22Q mutation does not change the conformation of the Aβ (16). Since this mutation neutralizes the E22 side chain, the electrostatic interactions involving E22 is supposed to be minor for the WT Aβ folding.

5.4. Importance of SLS to deposition

Both experimental (51,52) and theoretical (53) studies established a model for Aβ deposition. In this model, an Aβ monomer first docks onto fibril ends and then undergoes a conformational rearrangement into fibrillar structure. This is called two-stage dock-lock mechanism. The rearrangement of Aβ conformation in the lock stage is the rate-determining step. Interestingly, recent MD studies by Thirumalai and co-workers suggested that an Aβ(16-22) monomer could even add to pre-structured oligomers by the same dock-lock mechanism (54). According to the model, an Aβ monomer has many conformations in rapid equilibrium, each of which can go through its own dock-lock pathway. Therefore, Aβ deposition is composed of many parallel dock-lock pathways involving different Aβ conformations. Deposition rate should be determined by the dominant pathways in which Aβ monomer conformations are stable and their rearrangements in the lock stage are fast. Thus, these monomer conformations may be important deposition intermediates.

Our previous (22) and the current studies have shown that a strand-loop-strand (SLS) structure has considerable stability for the wide type Aβ(10-35). This SLS structure also has considerable population at the conditions such as E22Q and/or D23N mutations (16,55) and high temperature (16,56), which are known to promote Aβ aggregation. More importantly, the overall topology of the SLS structure resembles the Aβ monomer conformation in fibrils, which has a bend in V25-G29, leading to anti-parallel contact between its two β-sheet regions V12-V24 and A30-V40 (48,49). It is not unreasonable to expect that such a SLS monomer conformation, after docking to preformed fibril end, can undergo a conformational change to lock into the fibril with a relatively lower barrier compared to other monomer conformations. Therefore, the SLS structure may be an intermediate that correlates with Aβ deposition activity (Figure 14).

Experiments demonstrated that the F19T mutation changes Aβ monomer conformations and abolishes Aβ deposition activity (15,16). Our current simulations indicate that the F19T mutation indeed causes a significant change in the conformational feature of Aβ(10-35) monomer. For the F19T mutant, both loop 22-28 and SLS structures are significantly reduced in population by about 4-5 fold, but loop 15-23 becomes dominant. Experiments by Esler *et al* also revealed that a cross linking between the sidechains of the residues 14 and 22 removes the deposition activity of the Aβ (10-35) (16), indicate that the loop 15-23 may not be an active deposition conformation. Therefore, the current simulation results are in accord with the above hypothesis that the SLS is an important deposition structure, which accommodates the experimental observation that F19T mutation abolishes Aβ deposition activity.

6. ACKNOWLEDGEMENTS

We are grateful to the Research Grants Council of Hong Kong (HKUST6083/02M, N-HKUST 623/04) and the National Science Foundation of China (20225312) for financial support of the research.

7. REFERENCES

1. B. A. Yanker: Mechanisms of neuronal degeneration in Alzeimer's disease. *Neuron* 16, 921-932 (1996)

2. D. J. Selkoe: Neuroscience-Alzheimer's disease: genotypes, phenotypes and treatments. *Science* 275, 630-631 (1997)

3. B. A. Yanker, L. K. Duffy and D. A. Kirschner: Neurotrophic and neurotoxic effects of amyloid-β protein: reversal by tachykinin neuropeptides. *Science* 250, 279-282 (1990)

4. C. Geula, C. K. Wu, D. Saroff, A. Lorenzo, M. L. Yuan and B. A. Yanker: Aging renders the brain vulnerable to amyloid β-protein neurotoxicity. *Nature Med* 4, 827-831 (1998)

5. A. C. McKee, N. W. Kowall, J. S. Schumacher and M. F. Beal: The neurotoxicity of amyloid β-protein in aged primates. Amyloid: *Int J Exp Clin Invest* 5, 1-9 (1998).

6. J. M. Mason, N, Kokkoni, K, Stott, A. J. Doing: Design strategies for anti-amyloid agents. Curr Opin Struct Biol 13, 526-532 (2003)

7. P. Frid, S. V. Anisimov and N. Popovic: Congo Red and protein aggregation in neurodegenerative diseases. *Brain Res Rev* 53, 135-160. (2007)

8. J. Hardy and D. J. Selkoe: The amyloid hypothesis of Alzheimer's disease: progress and problem on the road to therapeutics. *Science* 297, 353-356 (2002)

9. F. Y, G. P. Lim, A. N. Begum, O. J. Ubeda, M. R. Simmons, S. S. Ambegaokar, P. Chen, R. Kayed, C. G. Glabe, S. A. Frautschy and G. M. Cole: Curcumin inhibits formation of amyloid β oligomers and fibrils, binds plaques, and reduces amyloid in vivo. *J Biol Chem* 280, 5892-5901 (2005)

10. M. Necula, R. Kayed, S. Milton and C. G. Glabe: Small molecule inhibits of aggregation indicate that amyloid β oligomerization and fibrillization pathways are independent and distinct. *J Biol Chem* 282, 10311-10324 (2007)

11. D. M. Walsh, I. Klyubin, J. V. Fadeeva, W. K. Cullen, R. Anwyl, M. S. Wolfe, M. J. Rowan and D. J. Selkoe: Naturally secreted oligomers of amyloid β protein potently inhibit hippocampal long-term potentiation in vivo. *Nature* 416, 535-539 (2002)

12. E. M. Snyder, Y. Nong, C. G. Almeida, S. Pauls, T. Moran, E. Y. Choi, A. C. Nairn, M. W. Salter, P. J. Lombroso, G. K. Gouras and P. Greengard: Regulation of NMDA receptor trafficking by amyloid-β. *Nature Neurosci* 8, 1051-1058 (2005)

13. J. P. Lee, E. R. Stimson, J. R. Ghilardi, P. W. Mantyh, Y. -A. Lu, A. M. Felix, W. Llanos, A. Behbin, M. Cumming, M. V. Criekinge, W. Timms and J. E. Maggio: 1H NMR of Aβ amyloid peptide congeners in water solution: conformational changes correlate with plaque competence. *Biochemistry* 34, 5191-5200 (1995)

14. S. Zhang, K. Iwata, M. J. Lachenmann, J. W. Peng, S. Li, E. R. Stimson, Y.-A. Lu, A. M. Felix, J. E. Maggio and J. P. Lee: The Alzeimer's peptide Aβ adopts a collapsed coil structures in water. *J Struct Biol* 130, 130-141 (2000)

15. W. P. Esler, E. R. Stimson, J. R. Ghilardi, Y.-A. Lu, A. M. Felix, H. V. Vinters, P. W. Mantyh, J. P. Lee and J. E. Maggio: Point substitution in the central hydrophobic cluster of a human β-amyloid congener disrupts peptide folding and abolishes plaque competence. *Biochemistry* 35, 13914-13921 (1996)

16. W. P. Esler, A. M. Felix, E. R. Stimson, M. J. Lachenmann, J. R. Ghilardi, Y.-A. Lu, H. V. Vinters, P. W. Mantyh, J. P. Lee and J. E. Maggio: Activation barriers to structural transition determine deposition rates of Alzheimer's disease Aβ amyloid. *J Struct Biol* 130, 174-183 (2000)

17. L. Hou, H. Shao, Y. Zhang, H. Li, N. K. Menon, E. B. Neuhaus, J. M. Brewer, I.-J. L. Byeon, D. G. Ray, M. P. Vitek, T. Iwashita, R. A. Makula, A. B Przybyla and M. G. Zagorski: Solution NMR studies of the Aβ(1-40) and Aβ(1-42) peptides establish that the Met35 oxidation states affects the mechanism of amyloid formation. *J Am Chem Soc* 126, 1992-2005 (2004)

18. J. Jarvet, P. Damberg, K. Bodell, L. E. Goran Eriksson and A. Graslund: Reversible random coil to β-sheet transition and the early stage of aggregation of the Aβ(12-28) fragment from the Alzheimer's peptide. *J Am Chem Soc* 122, 4261-4268 (2000)

19. N. D. Lazo, M. A. Grant, M. C. Condron, A. C. Rigby and D. B. Teplow: On the nucleation of amyloid β-protein monomer folding. *Protein Sci* 14, 1581-1596 (2005)

20. B. Y. Ma and R. Nussinov: Simulations as analytical tools to understand protein aggregation and predict amyloid conformation. *Curr Opin Chem Biol* 10, 445-452 (2006)

21. F. Massi and J. E. Straub: Simulation study of the structure and dynamics of the Alzheimer's amyloid peptide congener in solution. *Biophys J* 81, 697-709 (2001)

22. W. Han and Y.-D. Wu: A strand-loop-strand structure is a possible intermediate in fibril elongation: long time simulations of amyloid-β peptide (10-35). *J Am Chem Soc* 127, 15408-15416 (2005)

23. B. Tarus, J. E. Straub and D. Thirumalai: Dynamics of Asp23-Lys28 salt-bridge formation in Aβ (10-35) monomers. *J Am Chem Soc* 128, 16159-16168 (2006)

24. A. Baumketner and J.-E. Shea: The structure of the Alzheimer amyloid β 10-35 peptide probed through replica-exchange molecular dynamics simulations in explicit solvent. *J Mol Biol* 366, 275-285 (2007)

25. I. Daidone, F. Somona, D. Roccatano, R. A. Broglia, G. Tiana, G. Colombo and A. D. Nola: β-harpin conformation of fibrillogenic peptides: structure and α-β transition mechanism revealed by molecular dynamics simulations. *Proteins* 57, 198-204 (2004)

26. L. Cruz, B. Urbanc, J. M. Borreguero, N. D. Lazo, D. B. Teplow and H. E. Stanley: Solvent and mutation effects on the nucleation of amyloid β-protein folding. *Proc Natl Acad Sci USA* 102, 18258-18263 (2005)

27. A. Baumketner, S. L. Bernstein, T. Wyttenbach, N. D. Lazo, D. B. Teplow, M. T. Bowers and J.-E. Shea: Structure of the 21-30 fragment of amyloid β-protein. *Protein Sci* 15, 1239-1247 (2006)

28. W. Chen, N. Mousseau and P. Derreumaux: The conformations of the amyloid-β (21-30) fragment can be described by three families in solution. *J Chem Phys* 125, 084911 (2006)

29. N. G. Sgourakis, Y. Yan, S. A. McCallum, C. Wang and A. E. Garcia: The Alzeimer's peptides Aβ40 and Aβ42 adopt distinct conformations in water: a combined MD/NMR study. *J Mol Biol* 368, 1448-1457 (2007)

30. Y. C. Xu, J. H. Shen, X. M. Luo, W. L. Zhu, K. X. Chen, J. P. Ma and H. L. Jiang Conformational transition of amyloid β-peptide. *Proc Natl Acad Sci USA* 2005, 5403-5407 (102)

31. I. A. Mastrangelo, M. Ahmed, T. Sato, W. Liu, C. Wang, P. Hough, S. O. Smith. High-resolution atomic force microscopy of soluble Aβ42 oligomers. *J Mol Biol* 358, 106-119 (2006)

32. N. S. de Groot, F. X. Aviles, J. Vendrell and S. Ventura: Mutagenesis of the central hydrophobic cluster in Aβ42 Alzheimer's peptide: side-chain properties correlate with aggregation propensities. *FEBS J* 273, 658-668 (2006)

33. W. P. Esler, E. R. Stimson, J. M. Jennings, H. V. Vinters, J. R. Ghilardi, J. P. Lee, P. W. Mantyh and J. E. Maggio: Alzheimer's disease amyloid propagation by a template dependent dock-lock mechanism. *Biochemistry* 39, 6288-6295 (2000)

34. A. P. Pawar, K. F. DuBay, J. Zurdo, F. Chiti, M. Vendruscolo and C. M. Dobson: Prediction of "aggregation-prone" and "aggregation-susceptible" regions in protein associated with neurodegenerative diseases. *J Mol Biol* 350, 379-392 (2005)

35. O. Gursky and S. Aleshkov: Temperature-dependent β-sheet formation in β-amyloid Aβ (1-40) peptide in water: uncoupling β-structure folding from aggregation. *Biochim Biophys Acta* 1476, 93-102 (2000).

36. H. J. C. Berendsen, D. van der Spoel and R. van Drunen: GROMACS-a message-passing parallel molecular dynamics implementation. *Comput Phys Commun* 91, 43-56 (1995)

37. P. E. Smith, W. F. van Gunsteren: Consistent dielectric-properties of the simple point-charge and extended simple point-charge water model at 277 and 300 K. *J Chem Phys* 100, 3169-3174 (1994)

38. B. Hess, H Bekker, H. J. C. Berendsen and J. G. E. M. Fraaije: LINCS: a linear constraint solver for molecular simulations. *J Comput Chem* 18, 1463-1472 (1997)

39. S. Miyamoto and P. A. Kollman: SETTLE-an analytical version of the shake and rattle algorithm for rigid water models. *J Comput Chem* 13, 952-962 (1992)

40. I. G. Tironi, R. Sperb, P. E. Smith and W. F. van Gunsteren: A generalized reaction field method for molecular-dynamics simulations. *J Chem Phys* 102, 5451-5459 (1995)

41. W. Han and Y.-D. Wu: Molecular dynamics studies of hexamers of amyloid-β peptide (16-35) and its mutants: influence of charge states on amyloid formation. *Proteins* 66, 575-517 (2007)

42. K. A. Feenstra, B. Hess and H. J. C. Berendsen: Improving efficiency of large time-scale molecular dynamics simulations of hydrogen-rich systems. *J Comput Chem* 20, 786-798 (1999)

43. H. J. C. Berendsen, J. P. M. Postma, W. F. van Gunsteren, A. Di Nola and J. R. Haak: Molecular dynamics with coupling to an external bath. *J Chem Phys* 81, 3684-3690 (1984)

44. D. van der Spoel, E. Lindahl, B. Hess, A. R. van Buuren, E. Apol, P. J. Meulenhoff,
D. P. Tieleman, A. L. T. M. Sijbers, K. A. Feenstra, R. van Drunen and H. J. C. Berendsen: GROMACS user manual, version 3.2. www.gromacs.org (2004)

45. G. A., Kaminski, R. A. Friesner, J. Tirado-Rives and W. L. Jorgensen: Evaluation and reparametrization of the OPLS-AA force field for proteins via comparison with accurate quantum chemical calculations on peptides. *J Phys Chem B* 105, 6474-6487 (2001)

46. W. L. Jorgenson, J. Chandrasekhar, J. D. Madura, R. W. Impey and M. L. Klein: Comparison of simple potential functions for simulating liquid water. *J Chem Phys* 79, 926-935 (1983)

47. T. Darden, D. York, and L. Pederson: Particle mesh Ewald- an Nlog(N) method for Ewald sums in large system. *J Chem Phys* 98, 10089-10092 (1993)

48. A. T. Petkova, Y. Ishii, J. J. Balbach, O. N. Antzutkin, R. D. Leapman, F. Delaglio and R. Tycko: A structural model for Alzheimer's β-amyloid fibrils based on experimental constraints from solid state NMR. *Proc Natl Acad Sci USA* 99, 16742-16747 (2002)

49. B. Ma and R. Nussinov: Stabilities and conformations of Alzheimer's β-amyloid peptide oligomers ($A\beta_{16-22}$, $A\beta_{16-35}$ and $A\beta_{10-35}$): Sequence effects. *Proc Natl Acad Sci USA* 99, 14126-14131 (2002)

50. S. zhang and J. P. Lee: Selectively ^{2}H-labeled Glu/Asp: application to pK_a measurement in amyloid-β peptide. *J. Peptide Res* 5, 1-6 (200)

51. W. P. Esler, E. R. Stimson, J. M. Jennings, H. V. Vinters, J. R. Ghilardi, J. P. Lee, P. W. Mantyh and J. E. Maggio: Alzheimer's disease amyloid propagation by a template-dependent dock-lock mechanism. *Biochemistry* 39, 6288-6295 (2000)

52. R. Wetzel: Kinetics and thermodynamics of amyloid fibril assembly. *Acc Chem Res* 39, 671-679 (2006)

53. F. Massi and J. E. Straub: Energy landscape theory for Alzheimer's amyloid β-peptide fibril elongation. *Proteins* 42, 217 (2001)

54. P. H. Nguyen, M. S. Li, G. Stock, J. E. Straub and D. Thirumalai: Monomer adds to performed structured oligomers of Aβ-peptides by a two-stage dock-lock mechanism. *Proc Natl Acad Sci USA* 104, 111-116 (2007)

55. W. E. van Nostrand, J. P. Melchor, H. S. Cho, S. M. Greenberg and G. W. Rebeck: Pathogenic effects of D23N Iowa mutant amyloid β-protein. *J Biol Chem* 276, 32860-32866 (2001).

56. Y. Kusumoto, A. Lomakin, D. B. Teplow and G. B. Benedek: Temperature dependence of amyloid β-protein fibrilization. *Proc Natl Acad Sci USA* 95, 12277-12282 (1998)

Key Words: Amyloid beta Peptide, Alzheimer's Disease, Molecular Dynamics, Mutation, F19T, Aggregation

Send correspondence to: Dr Yun-Dong Wu, Department of Chemistry, The Hong Kong University of Science & Technology, Clear Water Bay, Kowloon, Hong Kong, China, Tel: 00852-2358-7391, Fax: 00852-2358-1594, E-mail: chydwu@ust.hk

http://www.bioscience.org/current/vol13.htm